

Short Communication

Fine-tuning the Cross-Sectional Architecture of Antimony-doped Tin Oxide Nanofibers as Pt Catalyst Support for Enhanced Oxygen Reduction Activity

Shuxiao Chen^{1,2}, Hongda Du^{1,2}, Yiping Wei¹, Lingyi Peng¹, Yadong Li¹, Lin Gan^{1,*}, Feiyu Kang^{1,2,*}

¹ Division of Energy and Environment, Graduate School at Shenzhen, Tsinghua University, Shenzhen, 518055, PR China

² Guangdong Provincial Key Laboratory of Thermal Management Engineering & Materials, Graduate School at Shenzhen, Tsinghua University, Shenzhen, 518055, PR China

*E-mail: lgan@sz.tsinghua.edu.cn, fykang@sz.tsinghua.edu.cn

Received: 31 March 2017 / Accepted: 11 May 2017 / Published: 12 June 2017

We report the fabrication of electrospun antimony-doped tin oxides (ATO) nanofibers (NFs) with controlled cross-sectional architectures ranging from solid dense NFs via fiber-in-tube NFs to completely hollow tube-like NFs at otherwise constant conditions. These ATO NFs were further applied as catalyst supports on which Pt nanoparticles were electrodeposited. Our results show that the Pt nanoparticles deposited on the hollow ATO NFs exhibited a higher catalytic activity on oxygen reduction reaction compared to those supported on solid ATO NFs and conventional ATO powders. Transmission electron microscopy revealed that the Pt nanoparticles deposited on the hollow ATO NFs were spontaneously confined into the hollow channels of the NFs, which likely induced a nano-confinement effect and hence higher catalytic activity. Our results provide important insight into rational control of the mesostructures of metal oxides supported fuel cell catalysts for enhance catalytic properties.

Keywords: electrospun nanofibers; antimony-doped tin oxides ; Pt nanoparticles; oxygen reduction reaction; nano-confinement effect

1. INTRODUCTION

One of the main challenges for the commercialization of polymer-electrolyte-membrane fuel cells (PEMFCs) is to explore durably highly active electrocatalysts for the cathodic oxygen reduction reaction (ORR) [1]. While significant progress has been made recently in exploring highly active platinum-based ORR catalysts by engineering their surface structures and compositions [2-8], a

durably active ORR catalyst working at the highly oxidative and corrosive ORR condition remains a nontrivial task. High surface area carbon supports that are normally used in conventional supported Pt catalysts suffered from severe oxidization (to CO₂) under the harsh oxidative ORR environment,[9-12] which in turn led to detachment or coalescence of the supported Pt NPs and thus activity loss.[12-14] In this context, metal oxides, particularly conductive metal oxides (such as In-doped SnO₂, denoted as ITO), have been recently explored as anti-corrosive ORR catalyst support due to their high corrosion resistance as well as high electron conductivity [15-19]. Liu et al. has demonstrated that using ITO as the support significantly improved the electrochemical activity and stability of Pt catalysts.[20] Other doped SnO₂ (such as Nb and Sb, etc) have been also developed as an alternate durable catalyst support.[19, 21, 22]

To further enhance the catalytic performance of oxide-supported catalysts and inspired by earlier studies on one-dimensional nanostructured carbon support (e.g. carbon nanotubes and nanofibers),[23-26] one-dimensional metal oxide nanostructures have attracted considerable interests as new catalyst supports due to their three-dimensional porous conductive network for efficient mass and electron transport. For instance, electrospun Sb- or Nb-doped SnO₂ nanofibers (NFs) have been developed as highly durable catalyst support recently.[27, 28] Nevertheless, these electrospun oxide NFs generally showed various cross-sectional morphologies such as solid and hollow NFs depending on the content and the type of the dopant. The impact of the cross-sectional architectures of NF support on the catalytic activities still remains largely unexplored.

In this contribution, we report a facile approach to control the cross-sectional morphology of electrospun Sb-doped SnO₂ (ATO) nanofibers at constant compositions and reveal how cross-sectional morphologies of the ATO NFs can impact on the electrocatalytic activity of supported Pt catalysts. This was achieved by controlling the heating rate during the calcination of precursor NFs at otherwise identical conditions. By electrodeposition, we found that Pt catalyst NPs can be spontaneously deposited inside the hollow channels of the hollow ATO NFs, leading to substantially enhanced ORR activity than those supported on the surface of solid NFs. Our results reveal a pronounced impact of the cross-sectional morphology of ATO NF support on the Pt catalytic activity and provide more rational design of 1D metal oxide NF as catalyst support.

2. EXPERIMENTAL

2.1. Materials

N,N-dimethylformamide (DMF), ethanol (C₂H₆O), toluene (C₇H₈), benzyl alcohol (C₇H₈O), acetone (C₃H₆O), stannous chloride dihydrate (SnCl₂·2H₂O), stannic chloride pentahydrate (SnCl₄·5H₂O), antimony trichloride (SbCl₃) were purchased from Sinopharm Chemical Reagent Co., Ltd. Polyvinylpyrrolidone (PVP, Mw~1300000) was purchased from Aladdin. Antimony triacetate (Sb(Ac)₃) was purchased from Sigma-Aldrich.

2.2. Preparation of electrospun ATO NFs

The precursor for electrospinning of ATO NFs was prepared by dissolving 5.3 mmol $\text{SnCl}_2 \cdot 2\text{H}_2\text{O}$ and 0.26 mmol of $\text{Sb}(\text{Ac})_3$ (i.e., at a nominal metal composition of $\text{SnSb}_{0.05}$) in 5 mL ethanol and 5 mL *N,N*-dimethylformamide (DMF), in which 1.20 g polyvinyl pyrrolidone (PVP, $M_w \sim 1300000$) was subsequently added and then stirred for 12 h. Single needle electrospinning was then conducted at a voltage of 21 kV and a distance of 15 cm between the needle and the collector. The obtained electrospun NFs were then calcined at 600 °C for 3 h in air at different heating rates (1, 5 and 10 °C/min) to form ATONFs with different cross-sectional morphologies.

For comparison, ATO NP aggregate powder with the same nominal metal composition of $\text{SnSb}_{0.05}$ were prepared by a solvothermal process.[29] In brief, $\text{SnCl}_4 \cdot 5\text{H}_2\text{O}$ (4.313 g) and SbCl_3 (0.148 g) were dissolved in mixed solution of toluene (10 ml) and benzyl alcohol (30 ml). Then, solution was heated in autoclave at 150 °C for 3 h. The obtained ATO NP powder was washed three times in acetone and then calcined at 500 °C for 1 h in air.

2.3. Electrodeposition of Pt catalyst on ATO NFs and ATO powder

Prior to electrodeposition, 2.0 mg ATO NFs (or ATO powder) were homogeneously dispersed in 1 mL isopropanol/ H_2O ($v/v = 1/4$) mixed solution containing 8 μL Nafion (5%) by ultrasonication for 10 minutes. A 10 μL portion of the solution was then casted onto a 5 mm-in-diameter glassy carbon electrode and dried at 50 °C in oven for 15 min, leading to a NF loading of 100 $\mu\text{g}/\text{cm}^2$. The Pt nanoparticles (NPs) were then electrodeposited on different ATO NF electrode in a N_2 -saturated 50 mM H_2SO_4 solution containing 1.0 mM H_2PtCl_6 . A Pt gauze and a mercurous sulfate electrode (MSE) were used as the counter and the reference electrode, respectively. Electrodeposition was performed by linear scanning voltammetry from 0.9 V to 0.24 V/RHE at 5 mV/s and kept at 0.24 V/RHE until a total charge of 38 mC achieved, leading to a Pt loading of 100 $\mu\text{g}/\text{cm}^2$ on the electrode (corresponding to a Pt content of 50 wt% in the supported catalysts). [30] The obtained electrodeposited Pt nanoparticles on the solid ATO NFs are denoted as Pt/ATO-sNF, the “fiber-in-tube” hollow ATO NFs are denoted as Pt/ATO-hNF, and the ATO powder support is denoted as Pt/ATO-P.

2.4. Materials Characterization

The morphologies of the nanofibers were characterized by field-emission scanning electron microscope (SEM) at an acceleration voltage of 15 kV. Transmission electron microscopy (TEM) and scanning TEM (STEM) were conducted on a 300 kV field-emission transmission electron microscope equipped with high angle annular dark field detector (HAADF) and energy-dispersive X-ray spectroscope (EDX). X-ray Diffraction (XRD) analysis were conducted using $\text{CuK}\alpha$ radiation at a voltage of 40 kV and a current of 100 mA. Thermal Gravimetric Analysis (TGA) and Differential Scanning Calorimetry (DSC) performed in air up to 800 °C at a heating rate of 10 °C/min.

2.5. Electrochemical measurements

The electrochemical surface area of the supported Pt catalyst was measured by cyclic voltammetry (CV) between 0.05~1.2 V/RHE at 100 mV/s in N₂-saturated 0.1 M HClO₄ solution. The ORR measurements were performed on a rotating disk electrode configuration at 1600 rpm which underwent linear sweep voltammetry (LSV) from 0.05 to 1.0 V/RHE at a scanning rate of 5 mV/s in O₂-saturated 0.1 M HClO₄ solution.

3. RESULTS AND DISCUSSION

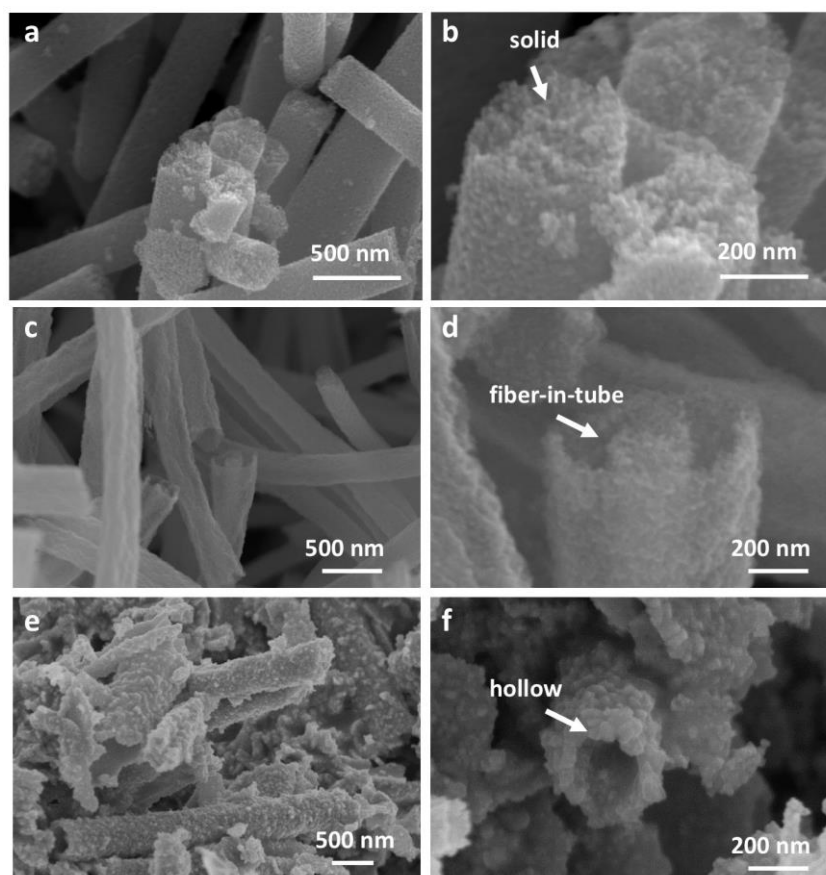


Figure 1. SEM images of solid dense (a, b), fiber-in-tube (c, d), and completely hollow (e, f) ATO NFs obtained by calcination of the electrospun SnCl₄/Sb(Ac)₃/PVP NF precursor from RT to 600 °C at a heating rate of 1°C/min, 5°C/min, and 10°C/min, respectively.

The ATO NFs were prepared by single-needle electrospinning of SnCl₂/Sb(Ac)₃/PVP precursor followed by calcination at 600°C in air for 3 h. The precursor NFs show a smooth surface and in the diameter mainly between 500 nm and 1 μm (Fig. S1). During the calcination, the PVP component was removed at around 300 °C - 600 °C as revealed by thermal gravimetric analysis combined with differential scanning calorimetry (Fig S2); meanwhile, the Sb(Ac)₃/SnCl₂ precursor was decomposed

and oxidized, leaving the ATO NF formed. Importantly, we found that the heating rate at the calcination step played an important role in fine-tuning the cross-sectional morphologies of the ATO NFs. Figure 1 present the SEM micrographs of the different ATO NFs obtained by calcination at a heating rate of 1, 5 and 10 °C/min, respectively, while keeping other conditions constant. At a very slow heating rate of 1°C/min, solid dense ATO NFs formed (Fig. 1a) and are found to be composed of primary ATO nanoparticles with size of ca. 10 nm (Fig. 1b). When calcined at 5°C/min, the obtained ATO NFs (Fig. 1 c, d) exhibited an unexpected fiber-in-tube hollow architecture as indicated by the open NF tip in Fig. 1d. Finally, calcination at 10°C/min led to the formation of completely hollow ATO NFs (Fig. 1e, f). A higher magnification of the SEM images indicates that these ATO NFs are also composed of aggregated primary NPs (Fig. 1d, f). Despite different morphologies, the different ATO NFs show a constant $\text{SnSb}_{0.05\pm 0.01}\text{O}_x$ compositions as confirmed by large area EDX, consistent with the nominal composition in the metal precursors. To the best of our knowledge, this is the first report on the preparation of doped SnO_2 NFs with controlled cross-sectional morphologies while at constant compositions.

For comparison, we have also prepared conventional ATO nanoparticle (NP) aggregate powder with the same Sn/Sb composition using a previously-reported solvothermal method (see SEM images in Fig. S3).[29] X-ray diffraction analysis(Fig. 2) shows that all the ATO NFs and the ATO NP powder have the same tetragonal cassiterite structure. No peaks of antimony oxide phase are found, indicating the insertion of Sb into the SnO_2 lattice. The average crystallite size derived from the diffraction peaks using Scherer's equation are also similar for different ATO NFs (ca. 10 nm), slightly larger than that of the ATO NP powder (ca. 5 nm).

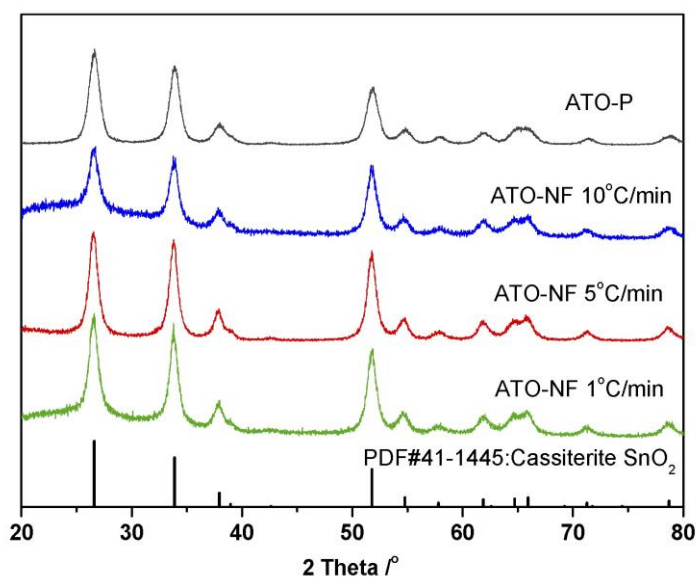


Figure 2. XRD patterns of different ATO NFs and ATO NP powder.

The formation of hollow metal oxide NFs during calcination of electrospun precursor NFs has been previously reported and was generally ascribed to a dominant Kirkendall effect combined with a

gas releasing effect.[27, 28, 31-34] The gas releasing effect is due to the fast decomposition of the polymer component (PVP) at high heating rates and high PVP contents, causing an increase of the pressure inside the fibers and thus the formation of hollow fibers. Below a certain weight content threshold ($\text{PVP}:\text{SnCl}_2\cdot 2\text{H}_2\text{O}=1.33$), however, only solid dense SnO_2 NFs were obtained.[33, 34] Since the PVP content ($\text{PVP}:\text{SnCl}_2\cdot 2\text{H}_2\text{O}=1$) used here is well below the threshold, the gas releasing effect may contribute to yet cannot fully accounts for the formation of hollow ATO NFs. The Kirkendall effect is associated with the outward diffusion of metal precursors from the center to the surface of the NFs during calcination. By tuning the content of SnO_2 with Nb or Sb,[27, 28] Cavaliere et al. obtained fiber-in-tube or hollow doped- SnO_2 NFs due to dopant-enhanced Kirkendall effect; a higher dopant content resulted in a higher percentage of the fiber-in-tube hollow NFs. Instead of tuning the dopant content, our results suggest that the heating rate may be an alternate tool to control the extent of Kirkendall effect. Slow heating rates ($1^\circ\text{C}/\text{min}$) resulted in slowly increased temperature and thereby slow atomic diffusion of salt precursors and a milder Kirkendall effect leading solid NFs, while calcination at higher heating rates ($5^\circ\text{C}/\text{min}$ and $10^\circ\text{C}/\text{min}$) rendered the temperature increasing quickly, favoring faster diffusion of metal precursors, stronger Kirkendall effect and thus the formation of fiber-in-tube or even completely hollow NFs (as schemed in Fig. 3). Additionally, the fast gas expansion at high heating rates may contributed to the formation of hollow NFs evidenced by the formation of some broken tube-like NFs in the SEM image (Fig. 1e). Overall, our results provide an easy-to-implement approach for fine-tuning the cross-sectional morphologies of ATO NFs at a constant doping composition.

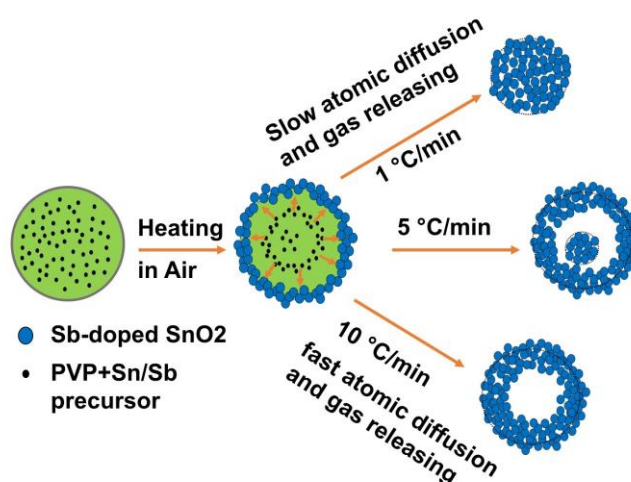


Figure 3. Illustration of the formation mechanism for ATO NFs with fine-tuned cross-sectional structures by combined Kirkendall effect and gas releasing effect depending on the heating rate.

To investigate the influence of the cross-sectional morphologies of ATO NFs on the electrocatalytic performance of supported catalysts, we further electrodeposited Pt/ATO-sNF, Pt/ATO-hNF, and Pt/ATO-P. The completely hollow ATO NFs were not used due to their destructive

morphology; their synthesis needs further optimization. During the electrodeposition, the Pt loading on the ATO NF electrode was controlled by the total charge associated with the reduction of PtCl_6^{2-} to Pt, which was set to be identical for all samples and led to a Pt loading of $100\mu\text{g}/\text{cm}^2$ and 50 wt% Pt content in the supported catalysts.

Figure 4 present the HAADF-STEM and high resolution TEM(HRTEM) micrographs of the Pt/ATO-sNF (Fig. 4a-c) and Pt/ATO-hNF catalyst (Fig. 4d-e). Pt NP aggregates with the size of 100-300 nm are clearly evident on both solid and the hollow “fiber-in-tube” ATO NFs. HRTEM shows that these Pt aggregates are composed of primary Pt nano crystallines with the size of 2-3 nm (Fig. 4b-c). Further optimization of the electrodeposition method is needed to improve the spatial distribution of Pt NPs. Interestingly, the majority of Pt NPs on the “fiber-in-tube” ATO NFs were spontaneously deposited inside the hollow channel of the support; few Pt NPs were found on the out walls (Fig. 4 d and e). While the detailed mechanism for the preferred deposition inside the fiber-in-tube ATO NFs needs further studies, it may be rationalized by a lower nucleation energy on the concave inner wall compared to the convex outer walls according to heterogeneous nucleation theory.[35]

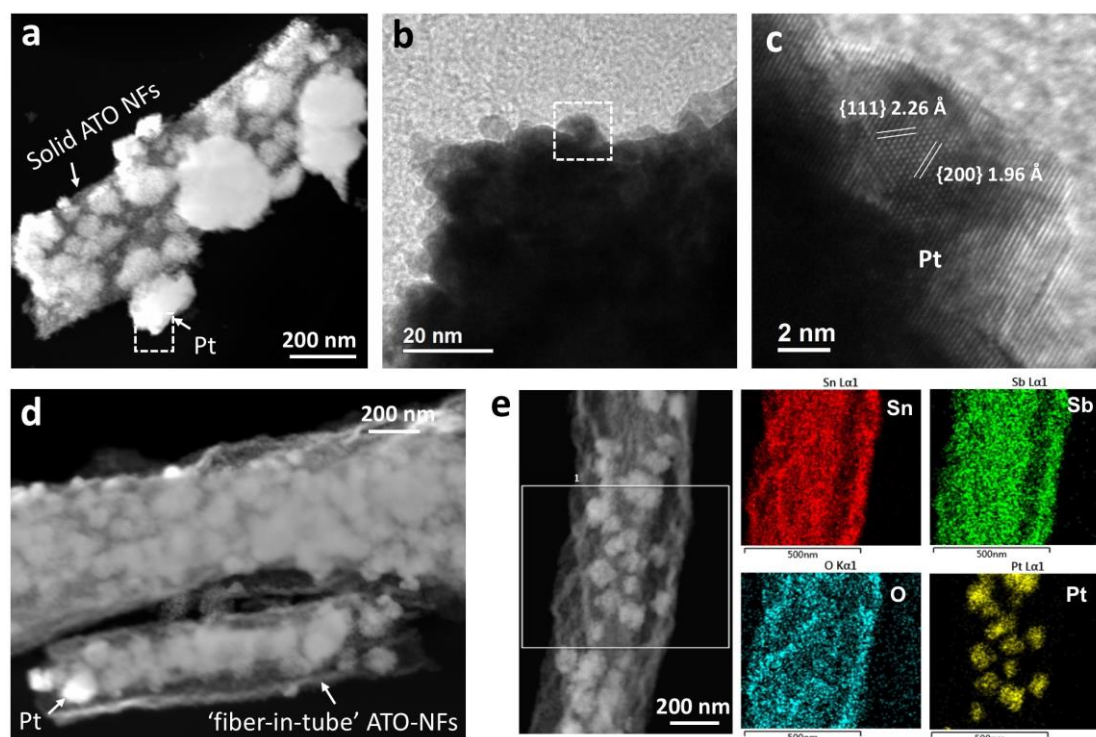


Figure 4. Microscopic characterization of Pt/ATO-sNF (a-c) and Pt/ATO-hNF (d-e) catalyst. (a) HAADF-STEM image of Pt/ATO-sNF catalyst. (b, c) High resolution TEM image of the Pt NP agglomerates as indicated in the dash box in (a). (d) HAADF-STEM image of the Pt/ATO-hNF catalyst, showing the preferential deposition of Pt NPs inside the hollow channel. (e) STEM-EDX elemental mapping of the of Pt/ATO-hNF catalyst.

Figure 5a shows the CVs of Pt/ATO-hNF, Pt/ATO-sNF, and Pt/ATO-P catalysts in N_2 -saturated 0.1 M HClO_4 solution at a scan rate of 100 mV/s, from which the calculated electrochemical

surface area (ECSA) of Pt are 15.1, 16.4 and 16.6 $\text{m}^2/\text{g}_{\text{Pt}}$, respectively. The somehow lower ECSA compared to the widely reported commercial Pt/C catalysts (usually around $60\text{m}^2/\text{g}_{\text{Pt}}$) is intrinsically tied to significant agglomeration of the electrodeposited Pt NPs; further optimization of the electrodeposition techniques is needed. Nevertheless, we can still observe a strong effect of the morphology of the ATO support on the ORR activities, as shown by their different ORR polarization curves in Fig. 5b. The Pt/ATO-hNF catalyst exhibits a high specific activity of $0.38\text{ mA}/\text{cm}^2_{\text{Pt}}$ at $0.9\text{V}/\text{RHE}$, significantly higher compared to Pt/ATO-sNF ($0.25\text{ mA}/\text{cm}^2_{\text{Pt}}$) and Pt/ATO-P ($0.12\text{ mA}/\text{cm}^2_{\text{Pt}}$) catalyst.

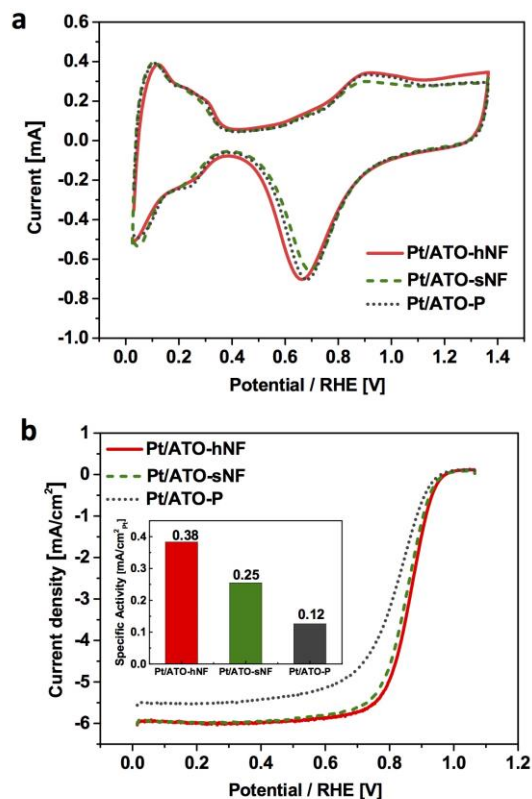


Figure 5. Electrochemical measurement of Pt/ATO-hNF, Pt/ATO-sNF and Pt/ATO-P catalyst: (a) CV curves of in N_2 -saturated 0.1 M HClO_4 solution at a scanning rate of $100\text{ mV}/\text{s}$. (b) ORR polarization curves measured on RDE rotated at 1600 rpm in O_2 saturated 0.1 M HClO_4 solution at a scanning rate of $5\text{ mV}/\text{s}$. The inset compares their intrinsic specific activities at $0.9\text{V}/\text{RHE}$.

The enhanced ORR activity on the Pt/ATO-hNF catalyst compared to the Pt/ATO-sNF and Pt/ATO-P catalyst despite their same Pt loadings and similar Pt NP sizes indicates a pronounced morphological effect of the ATO support on the ORR electrocatalysis. Firstly, the one-dimensional nanostructure of the ATO NFs constitutes a 3D conductive network leading to high electron conductivity and favoring a higher activity, which has been demonstrated in previous studies using carbon nanotubes/nanofibers as catalyst support.[24-26] Secondly and more interestingly, confining Pt NPs in the hollow channel of the fiber-in-tube ATO NFs resulted in further enhancement compared to

those supported on the out surface of the solid ATO NFs. This may be ascribed to enhanced collision probability of the O₂ molecule on the catalytic Pt surface inside the hollow channels of the fiber-in-tube ATO NFs, an effect that has been previously reported as the ‘nano-confinement effect’ for catalysts confined inside carbon nanotube supports during gas phase catalytic reactions such as ethanol production from CO and ammonium decomposition.[36, 37] Our study suggests that the hollow channel of the fiber-in-tube ATO-NFs may also bring in similar nano-confinement effect on the Pt catalysts for the liquid phase electrocatalytic reduction of oxygen molecule, leading to the further improvement on the ORR activity. This result provides a new way to improve the ORR activity of the metal oxide supported fuel cell electrocatalysts.

4. CONCLUSION

We report the controlled synthesis of electrospun ATO NFs with distinct cross-sectional morphologies including solid dense NFs, fiber-in-tube NFs and completely hollow NPs by controlling the heating rate during calcination step while keeping their phase and composition constant. By electrodeposition, we found that Pt NPs were spontaneously deposited inside the hollow channels of the fiber-in-tube ATO NFs, showing substantially enhanced ORR activity compared to those deposited on the out surfaces of solid ATO NFs as well as those supported on conventional ATO NP aggregates. Our result suggests that the previously-established confinement effect for enhancing catalytic activities at solid/gas interfaces can be also applied to the ORR electrocatalysis at the solid/liquid interfaces. The hollow ATO NFs with their inner channels provide as a promising catalyst support bearing this confinement effect. These results provide important insight into rational control of mesostructures of ATO supports to achieve both high activity and high durability of fuel cell catalyst.

SUPPLEMENTARY FIGURES

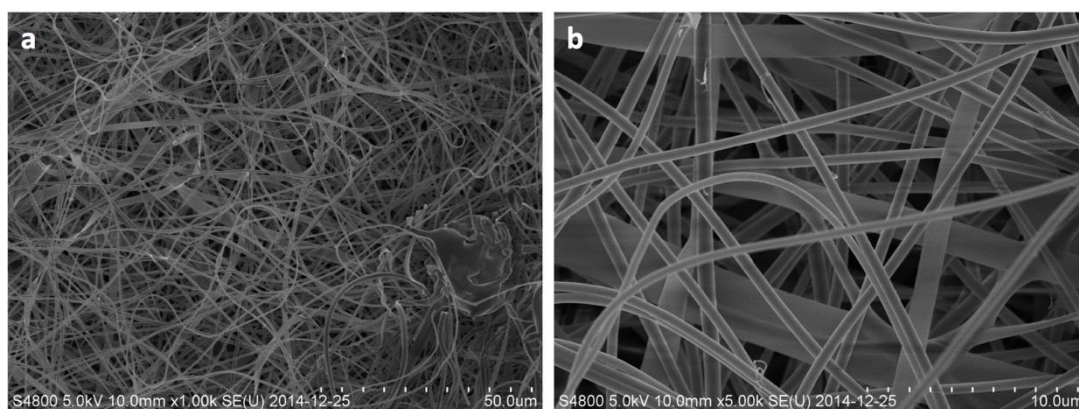


Figure S1. SEM images of the electrospun SnCl₂/Sb(Ac)₃/PVP nanofibers

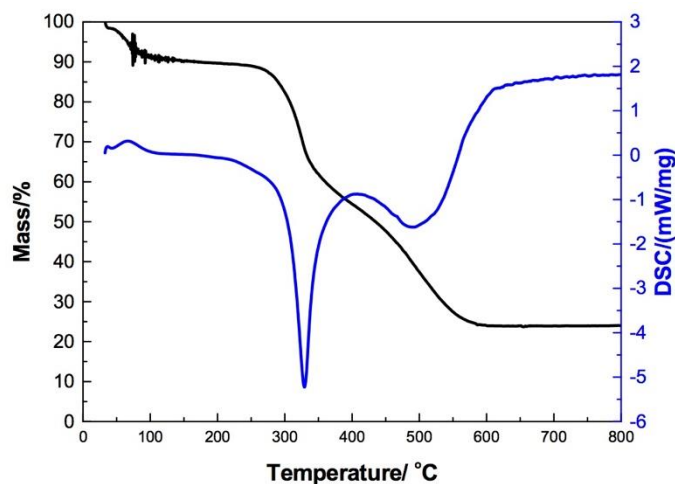


Figure S2. Thermal gravimetric analysis and differential scanning calorimetry of electrospun $\text{SnCl}_2/\text{Sb}(\text{Ac})_3/\text{PVP}$ nanofibers

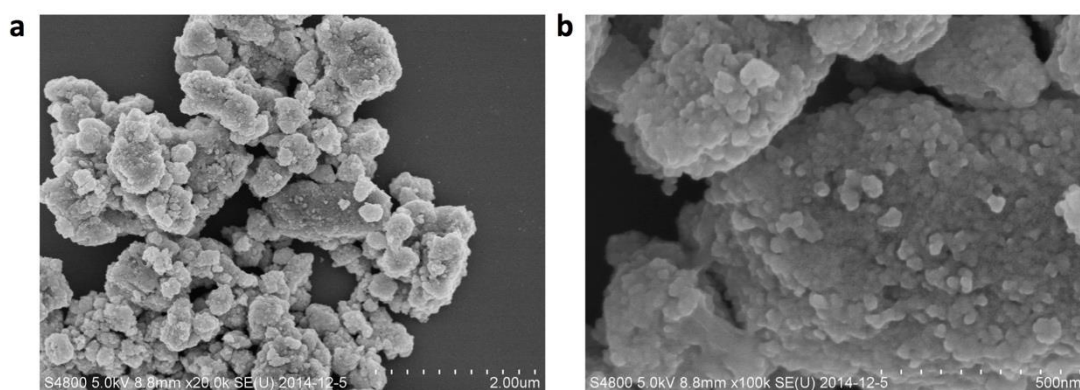


Figure S3. SEM image of ATO nanoparticle aggregates

ACKNOWLEDGMENT

This work was supported by the National Key Basic Research Program of China (No.2014CB932400), Guangdong Natural Science Foundation for Distinguished Young Scholars (2016A030306035) and Shenzhen City Technology Innovation Committee (JCYJ20160531194754308, JCYJ20140902110354242, JC201105201119A, and ZDSYS20140509172959968).

References

1. M. K. Debe, *Nature* 486 (2012) 43.
2. D. Wang, H. L. Xin, R. Hovden, H. Wang, Y. Yu, D. A. Muller, F. J. DiSalvo and H. D. Abruna, *Nat. Mater.* 12 (2013) 81.
3. C. Cui, L. Gan, M. Heggen, S. Rudi and P. Strasser, *Nat. Mater.* 12 (2013) 765.
4. C. Chen, Y. Kang, Z. Huo, Z. Zhu, W. Huang, H. L. Xin, J. D. Snyder, D. Li, J. A. Herron, M. Mavrikakis, M. Chi, K. L. More, Y. Li, N. M. Markovic, G. A. Somorjai, P. Yang and V. R. Stamenkovic, *Science* 343 (2014) 1339.
5. L. Gan, C. Cui, M. Heggen, F. Dionigi, S. Rudi and P. Strasser. *Science* 346 (2014) 1502.
6. X. Huang, Z. Zhao, L. Cao, Y. Chen, E. Zhu, Z. Lin, M. Li, A. Yan, A. Zettl, Y. M. Wang, X. Duan,

- T. Mueller and Y. Huang, *Science* 348 (2015) 1230.
7. L. Gan, M. Heggen, C. H. Cui and P. Strasser, *ACS Catal.* 6 (2016) 692.
 8. L. Zhang, L. T. Roling, X. Wang, M. Vara, M. Chi, J. Liu, S.-I. Choi, J. Park, J. A. Herron, Z. Xie, M. Mavrikakis and Y. Xia, *Science* 349 (2015) 412.
 9. S. D. Knights, K. M. Colbow, J. St-Pierre and D. P. Wilkinson, *J. Power Sources* 127 (2004) 127.
 10. J. Wang, G. Yin, Y. Shao, S. Zhang, Z. Wang and Y. Gao, *J. Power Sources* 171 (2007) 331.
 11. X. Yu and S. Ye, *J. Power Sources* 172 (2007) 133.
 12. E. Antolini, *J. Mater. Sci.* 38 (2003) 2995
 13. Y. Shao, G. Yin and Y. Gao, *J. Power Sources* 171 (2007) 558.
 14. X. Yu and S. Ye, *J. Power Sources* 172 (2007) 145.
 15. E. Antolini and E. R. Gonzalez, *Solid State Ionics* 180 (2009) 746.
 16. Y. Shao, J. Liu, Y. Wang and Y. Lin, *J. Mater. Chem.* 19 (2009) 46.
 17. Z. Zhang, J. Liu, J. Gu, L. Su and L. Cheng, *Energy Environ. Sci.* 7 (2014) 2535.
 18. H. Lv and S. Mu, *Nanoscale* 6 (2014) 5063.
 19. D. J. You, K. Kwon, C. Pak and H. Chang, *Catal. Today.* 146 (2009) 15.
 20. Y. Liu and W. E. Mustain, *J. Am. Chem. Soc.* 135 (2013) 530.
 21. F. Takasaki, S. Matsuie, Y. Takabatake, Z. Noda, A. Hayashi, Y. Shiratori, K. Ito and K. Sasaki, *J. Electrochem. Soc.* 158 (2011) B1270.
 22. K. Kakinuma, Y. Chino, Y. Senoo, M. Uchida, T. Kamino, H. Uchida, S. Deki and M. Watanabe, *Electrochim. Acta* 110 (2013) 316.
 23. W. Z. Li, C. H. Liang, J. S. Qiu, W. J. Zhou, H. M. Han, Z. B. Wei, G. Q. Sun and Q. Xin, *Carbon* 40 (2002) 791.
 24. L. Gan, R. Lv, H. Du, B. Li and F. Kang, *Carbon* 47 (2009) 1833.
 25. L. Gan, H. Du, B. Li and F. Kang, *Chem. Commun.* 47 (2011) 3900.
 26. R. Lv, T. Cui, M.-S. Jun, Q. Zhang, A. Cao, D. S. Su, Z. Zhang, S.-H. Yoon, J. Miyawaki, I. Mochida and F. Kang, *Adv. Funct. Mater.* 21 (2011) 999.
 27. S. Cavaliere, I. Jimenez-Morales, G. Ercolano, I. Savych, D. Jones and J. Roziere, *Chemelectrochem* 2 (2015) 1966.
 28. S. Cavaliere, S. Subianto, I. Savych, M. Tillard, D. J. Jones and J. Roziere, *J. Phys. Chem. C* 117 (2013) 18298.
 29. V. Muller, M. Rasp, G. Stefanic, J. Ba, S. Guenther, J. Rathousky, M. Niederberger and D. Fattakhova-Rohlfing, *Chem. Mater.* 21 (2009) 5229.
 30. A. L. Santos, D. Profeti and P. Olivi, *Electrochim Acta* 50 (2005) 2615.
 31. Y. Cheng, W. Huang, Y. Zhang, L. Zhu, Y. Liu, X. Fan and X. Cao, *Crystengcomm* 12 (2010) 2256.
 32. X. Xia, X. J. Dong, Q. F. Wei, Y. B. Cai and K. Y. Lu, *Express Polymer Letters* 6 (2012) 169.
 33. C. Gao, X. Li, B. Lu, L. Chen, Y. Wang, F. Teng, J. Wang, Z. Zhang, X. Pan and E. Xie, *Nanoscale* 4 (2012) 3475.
 34. L. Li, X. Yin, S. Liu, Y. Wang, L. Chen and T. Wang, *Electrochem. Commun.* 12 (2010) 1383.
 35. M. Qian and J. Ma, *J. Crystal Growth* 355 (2012) 73.
 36. X. Pan, Z. Fan, W. Chen, Y. Ding, H. Luo and X. Bao, *Nat. Mater.* 6 (2007) 507.
 37. J. Zhang, J.-O. Müller, W. Zheng, D. Wang, D. Su and R. Schlögl, *Nano. Lett.* 8 (2008) 2738.